Available online at www.sciencedirect.com

SciVerse ScienceDirect

Ceramics International 39 (2013) 4877–4886

CERAMICS INTERNATIONAL

www.elsevier.com/locate/ceramint

Morphotropic phase boundary and electrical properties of $1-x[Bi_{0.5}Na_{0.5}]TiO_3-xBa[Zr_{0.25}Ti_{0.75}]O_3$ lead-free piezoelectric ceramics

B. Parija[a], T. Badapanda[b,*], S.K. Rout[c], L.S. Cavalcante[d,e], S. Panigrahi[a], E. Longo[d], N.C. Batista[e], T.P. Sinha[f]

[a]*Department of Physics, NIT, Rourkela 769008, India*
[b]*Department of Physics, CV Raman College of Engineering, Bhubaneswar 752054, India*
[c]*Department of Applied Physics, BIT, Meshra, Ranchi, India*
[d]*Universidade Estadual Paulista, PO Box 355, CEP 14801-907, Araraquara-SP, Brazil*
[e]*UESPI, CCN, Departamento de Química, Rua João Cabral, PO Box 2231, 64002-150 Teresina-PI, Brazil*
[f]*Department of Applied Physics, Bose Institute, 93/1, A.P.C. Road, Kolkata 700009, India*

Received 27 September 2012; received in revised form 15 November 2012; accepted 23 November 2012
Available online 5 December 2012

Abstract

Lead-free solid solutions $(1-x)Bi_{0.5}Na_{0.5}TiO_3$ (BNT)–$xBaZr_{0.25}Ti_{0.75}O_3$ (BZT) ($x=0$, 0.01, 0.03, 0.05, and 0.07) were prepared by the solid state reaction method. X-ray diffraction (XRD) and Rietveld refinement analyses of $1-x$(BNT)–x(BZT) solid solution ceramic were employed to study the structure of these systems. A morphotropic phase boundary (MPB) between rhombohedral and cubic structures occured at the composition $x=0.05$. Raman spectroscopy exhibited a splitting of the (TO_3) mode at $x=0.05$ and confirmed the presence of MPB region. Scanning electron microcopy (SEM) images showed a change in the grain shape with the increase of BZT into the BNT matrix lattice. The temperature dependent dielectric study showed a gradual increase in dielectric constant up to $x=0.05$ and then decrease with further increase in BZT content. Maximum coercive field, remanent polarization and high piezoelectric constant were observed at $x=0.05$. Both the structural and electrical properties show that the solid solution has an MPB around $x=0.05$.

Keywords: C. Electrical property; Rietveld refinement; Raman spectroscopy; Phase boundaries

1. Introduction

Lead based piezoelectric ceramics are widely applied in electronic and microelectronic devices due to their excellent piezoelectric properties. However, the toxicity of lead oxide and its high vapor pressure during sintering processing cause serious environmental problem. So there is a huge demand of lead-free piezoelectric ceramic materials for various technological applications. Several works have been reported on the electrical properties of lead-free piezoelectric ceramics [1–4]. Among the various lead-free ceramics bismuth sodium titanate (BNT) is considered as a potential candidate for applications in piezoelectric devices. This ceramic material exhibits strong ferroelectric properties with a relatively high Curie temperature. Moreover, the BNT-based materials possess an elevated anisotropic electromechanical coupling at a high frequency constant and lower dielectric constant [5] which justifies its applications in ultrasonic devices. Thus, the BNT-based ceramics have great prospects not only for environmental protection but also for different electronic applications.

The physical properties of BNT complex ceramic have been reported in 1961 by Smolenskii et al. [6]. Moreover it is also reported that this compound has a perovskite-type rhombohedral structure with formula (A'A'')BO_3 and space group ($R3c$) in the temperature range of 25–200 °C [7–12]. BNT exhibits a high coercivity ($E_c=73$ kV/cm), and considerable remanent polarization ($P_r=38$ μC/cm^2). This material is also mechanically tough, less toxic and also exhibits

*Corresponding author. Tel.: +919437306100; fax: +916612462999.
E-mail address: badapanda.tanmaya@gmail.com (T. Badapanda).

0272-8842/$ - see front matter © 2012 Elsevier Ltd and Techna Group S.r.l. All rights reserved.
http://dx.doi.org/10.1016/j.ceramint.2012.11.080

optical isotropism during the diffuse phase transition [13–17]. However, the major drawback of the BNT compound is its high conductivity. In order to obtain useful lead-free piezoelectric ceramic some modification in the BNT ceramic has been employed in the literature by diffusing with the other perovskites system to form solid solution [18–21]. Some recent works have been reported in the literature on the improvement of piezoelectric properties of BNT-based ceramics by making solid solutions [22–24]. This method is a trade-off to make use of the solid-solution technique to substitute the individuals and seek for the merits of the selected materials. $BaTiO_3$ and its doped species have been investigated to develop high-quality lead-free ceramics. It is observed that the substitution of Zr^{4+} ions by the Ti^{4+} ions in $BaTiO_3$ can significantly improve the overall properties of the material because of its better chemical stability [25]. The composition $Ba[Zr_{0.25}Ti_{0.75}]O_3$ (BZT) was chosen because it shows a diffuse phase transition behavior which is already reported by the author in a previous work [26].

Therefore in this paper, we report the structural and electrical properties of $1-x$(BNT)–x(BZT) solid solution emphasizing the presence of morphotropic phase boundary (MPB).

2. Experimental details

2.1. Synthesis of 1–x(BNT)–x(BZT) ceramics

$[Bi_{0.5}Na_{0.5}]TiO_3$ (BNT) and $Ba[Zr_{0.25}Ti_{0.75}]O_3$ (BZT) ceramics were prepared by the conventional solid state reaction method separately. Reagent grade oxide or carbonate powder of bismuth oxide Bi_2O_3 (Merck, India; 99.9%), sodium carbonate Na_2CO_3 (Merck, India; 99.9%), barium carbonate $BaCO_3$ (Loba Chem., India, 99.9%), zirconium oxide ZrO_2 (Merck, India, 99.9%) and titanium oxide TiO_2 (Merck, India, 99.9%) were used as starting raw materials. Stoichiometric amounts of the starting reagents were ball-milled in ethanol media for 12 h. BNT samples were heat-treated at 850 °C for 2 h with intermediate grinding and mixing. The BZT samples were heat-treated at 1200 °C for 4 h with intermediate grinding and mixing. Appropriate amounts of single phase BNT and BZT powders were grinded for 4 h adding 5% polyvinyl alcohol as a binder. The granules were sieved and uniaxially cold pressed with a load of 6 t to obtain discs with a diameter of about 10 mm. The discs were decarbonized at 550 °C and then sintered at 1150 °C for 4 h in a covered alumina crucible with Bi_2O_3 powder in the crucible.

2.2. Characterizations

The crystalline structure of $1-x$(BNT)$-x$(BZT) ceramic was analyzed by X-ray diffraction (XRD), (Xpert MPD, Philips, UK). The degree of structural order and phase solubility of the ceramic system was investigated by micro-Raman spectroscopy (ENWAVE OPTRONICS-EZRAMAN). The micro-Raman spectra were collected using an Ar^+ laser operated at excitation wavelength 633 nm. The microstructure of ceramics sintered at 1150 °C for 4hrs was observed by scanning electron microscopy (SEM) (JEOL: JSM 6480LV, Japan). Silver paste was applied to both faces followed by heat treatment of the samples at 500 °C (20 min) for electrical measurements. Evolutions of the relative permittivity (ε_r) and dissipation factor (tan δ) with temperature were measured from room temperature (30 °C) to 475 °C, using an LCR meter (Hioki, Japan) operated in the frequency range from 40 Hz to 1 MHz. The dielectric data were taken every 5 °C, keeping a heating rate of 1 °C/min. The polarization versus electric field (P–E) loops of the specimens, were studied using a modified radiant automatic P–E loop tracer circuit by applying AC field. The sintered ceramic samples were polarized in silicone oil at 100 °C under 35 kV/cm for 20 min and piezoelectric constant (d_{33}) values of the samples were measured using a piezo-d_{33} meter (YE2730A d_{33} meter).

3. Results and discussions

3.1. X-ray diffraction and Rietveld refinement analyses

Fig. 1a and b illustrates the XRD patterns of $1-x$(BNT)$-x$(BZT) ceramic with different compositions from 0 to 0.07 and reduced XRD patterns from 44° to 49° of these ceramics, respectively. The XRD patterns of all the $1-x$(BNT)$-x$(BZT) ceramics can be indexed to a perovskite-type rhombohedral structure with the space group ($R\bar{3}c$). Moreover, it is observed that all the compositions are of single phase without the presence of any deleterious phases (Fig. 1(a)). This indicates that the BZT ceramic diffuses completely into the BNT lattice matrix to form a homogeneous $1-x$(BNT)$-x$(BZT) ceramic solid solution. From the reduced XRD pattern as shown in Fig. 1(b), it is observed that there is no observable peak splitting for composition $x \leq 0.03$, indicating that these compositions have a pure rhombohedral symmetry. It is also observed that there is a shift in the peak towards the lower angle side indicating an increment in lattice parameter and cell volume with increase in BZT content due to the large radius of Ba^{2+} (1.61 Å) in relation to $[Bi_{0.5}Na_{0.5}]^{2+}$ (~1.40 Å) [27]. With further increase in x, the (024) peak tends to split and the splitting becomes more and more obvious, suggesting that a new cubic phase appears. However in the XRD patterns of $1-x$(BNT)$-x$(BZT) with $x=0.05$ it is observed that there is a considerable shift of angle (2θ) towards the higher side and consequently a reduction of lattice parameters.

The structural refinement of the $1-x$(BNT)$-x$(BZT) ceramics with different x compositions from 0 to 0.07 was performed by MAUD software (version 2.33) [28–30] employing the Rietveld refinement method [31]. The results obtained from the Rietveld refinement show good agreement between the measured experimental XRD patterns and theoretical line profile (Fig. 2(a, b); Supplementary data Fig S1 (a–d)). It is also observed that the profiles of

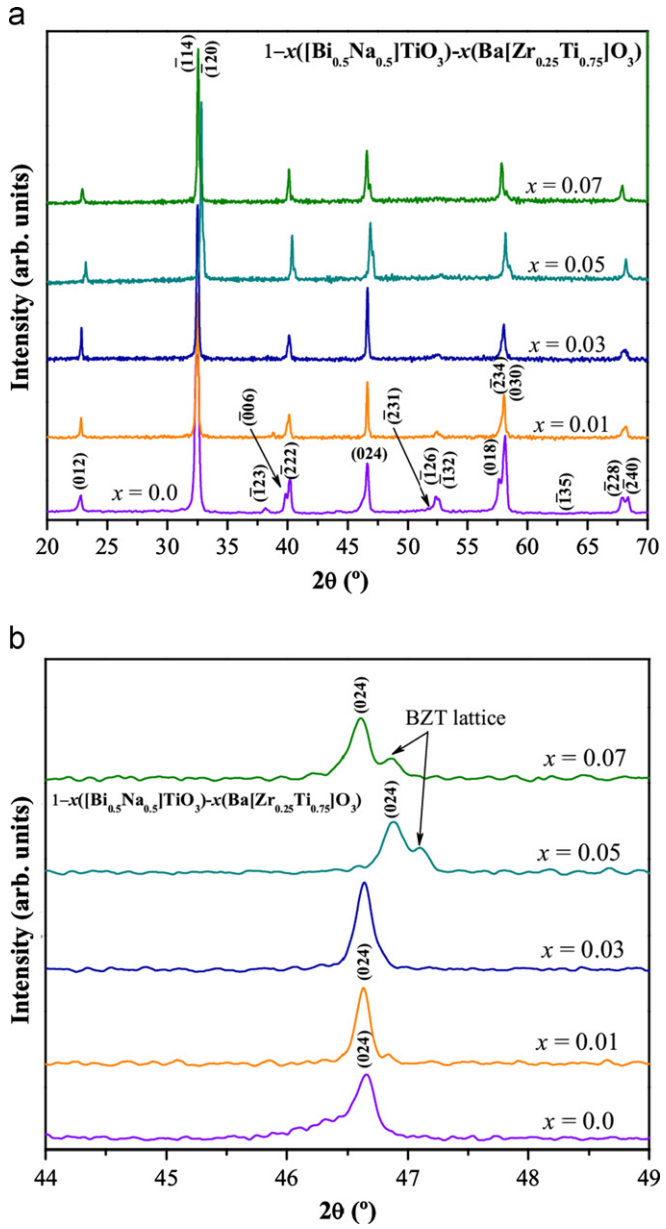

Fig. 1. (a) XRD patterns of $1-x(Bi_{0.5}Na_{0.5})TiO_3-xBa[Zr_{0.25}Ti_{0.75}]O_3$ ceramics and (b) XRD patterns in the range from 44° to 49°.

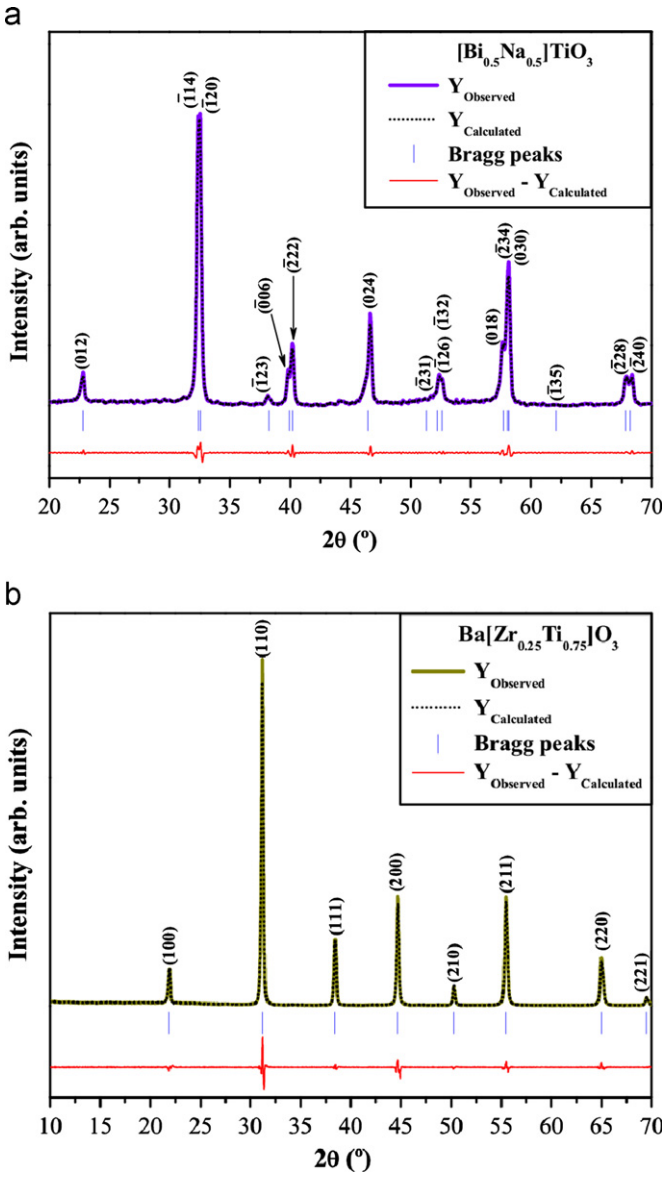

Fig. 2. Rietveld refinement plots of: (a) $(Bi_{0.5}Na_{0.5})TiO_3$ and (b) $Ba[Zr_{0.25}Ti_{0.75}]O_3$ ceramics.

the XRD patterns experimentally observed and those theoretically calculated displays small difference as illustrated by a line $Y_{Observed}-Y_{Calculated}$. The lattice parameters and atomic positions obtained from the Rietveld refinement are listed in Table 1.

The fitting parameters (R_{wnb}, R_b, R_{exp}, R_w, and σ) suggest that the refinement results are reliable. In our work, the optimized parameters are scale factor, background with exponential shift, exponential thermal shift and polynomial coefficients, basic phase, microstructure, crystal structure, size-strain, structure solution model (genetic algorithm SDPD), shift lattice constants, profile half-width parameters (u, v, w), texture, lattice parameters (a, b, c), factor occupancy and atomic site occupancies (Wyckoff) [32,33].

In the Rietveld refinement, the measured diffraction patterns match the Crystallographic Information File (CIF) No. 154040 and 88533, for BNT and BZT structures, respectively [34,35]. In fact, the results arising from structural refinements are commonly acceptable under the following criteria: (a) $R_w < 10\%$—medium complex phases (tetragonal, orthorhombic, rhombohedral and hexagonal); (b) $R_w < 15\%$—high complex phases (monoclinic and triclinic) and (c) $R_w < 8\%$—cubic structure (high symmetry and few diffraction peaks). Also, low σ values (<2) indicate a good accuracy of the refinement results obtained [36]. Table 1 confirms a good fitting obtained with CIFs reported. These parameters were employed to model the unit cells of BNT and BZT ceramics by means of the visualization for electronic and structural analysis (VESTA) program (Version 3.1.0 for Windows) [37].

Table 1
Lattice parameters, unit cell volume, atomic coordinates and site occupation obtained by Rietveld refinement data for the $(Bi_{0.5}Na_{0.5})TiO_3$ and $Ba[Zr_{0.25}Ti_{0.75}]O_3$ ceramics.

Atoms	Wyckoff	Site	x	y	z
Bi	6*a*	3.	0	0	0.212651
Na	6*a*	3.	0	0	0.286785
Ti	6*a*	3.	0	0.5	0.041088
O1	18*b*	1	0.0921515	0.177511	0.092341
$R\bar{3}c$ (161) – rhombohedral ($a=b=5.4629(3)$; $c=13.4835(4)$ Å; $c/a=2.4682$; $V=348.19$ Å^3) $R_p=9.82\%$; $R_{wp}=5.4\%$; $R_{exp}=2.2\%$ and $\sigma=2.45$					
Ba	1*a*	$m-3m$	0	0	0
Zr	1*b*	$m-3m$	0.5	0.5	0.5
Ti	1*b*	$m-3m$	0.5	0.5	0.5
O	3*c*	*mm*2.	0	0.5	0.5
$Pm\bar{3}m$ (221) – cubic ($a=b=c=4.0563(4)$ Å; $c/a=1$; $V=66.74$ Å^3) $R_p=3.97\%$; $R_{wp}=6.45\%$; $R_{exp}=2.6\%$ and $\sigma=2.48$					

3.2. Representation for the $(Bi_{0.5}Na_{0.5})TiO_3$ and $Ba[Zr_{0.25}Ti_{0.75}]O_3$ lattice

Fig. 3a and b show the representations of the BNT ($1\times1\times1$) unit cells and BZT supercells ($1\times2\times2$) respectively. Fig. 3(a) illustrates the unit cell for BNT ceramic with trigonal or rhombohedral structure, space group ($R\bar{3}c$), point-group symmetry (C_{3v}^6) and two molecular formula per unit cell ($Z=2$) [38]. In this unit cell, bismuth (Bi) and sodium (Na) atoms are coordinated to six oxygens (O) atoms, which form the distorted octahedral $[BiO_6]$ and $[NaO_6]$ clusters (6-vertices, 6-faces and 12-edges) [39]. In addition the titanium (Ti) atoms are hexacoordinated to six O atoms, represented by the octahedral $[TiO_6]$ clusters (Fig. 3(a)). Fig. 3(b) illustrates the presence of four unit cells forming the supercell ($1\times2\times2$) for the cubic structure of the BZT ceramic. This lattice has a space group ($Pm\bar{3}m$), point-group symmetry (O_h^1) and one molecular formula per unit cell ($Z=1$). In this supercell of BZT, barium (Ba) atoms are coordinated to twelve oxygens atoms which form the polyhedrons with cuboctahedral configuration for the $[BaO_{12}]$ clusters. The cuboctahedron has twelve identical vertices which are formed by the meeting of two triangles and two squares, fourteen faces and twenty-four identical edges, and each vertice separates a triangle from a square [40], while the Ti and Zr atoms are bonded to six O atoms to form a polyhedron (octahedron) which are written as $[TiO_6]$ and $[ZrO_6]$ clusters [39].

3.3. Raman spectra analyses

Fig. 4 elucidates the Raman spectroscopy study of $1-x$ (BNT)$-x$(BZT) ceramic with $x=0,0.01$, 0.03, 0.05 and 0.07. The rhombohedral structure of BNT has 13 Raman-active modes, which can be represented as $\Gamma_{Raman}=7A_1+6E$. However, Fig. 4 displays only five Raman-active modes in the range from 100 to 1,000 cm^{-1} which is in agreement with the works reported by Rout et al. [41] and Eerd et al. [42].

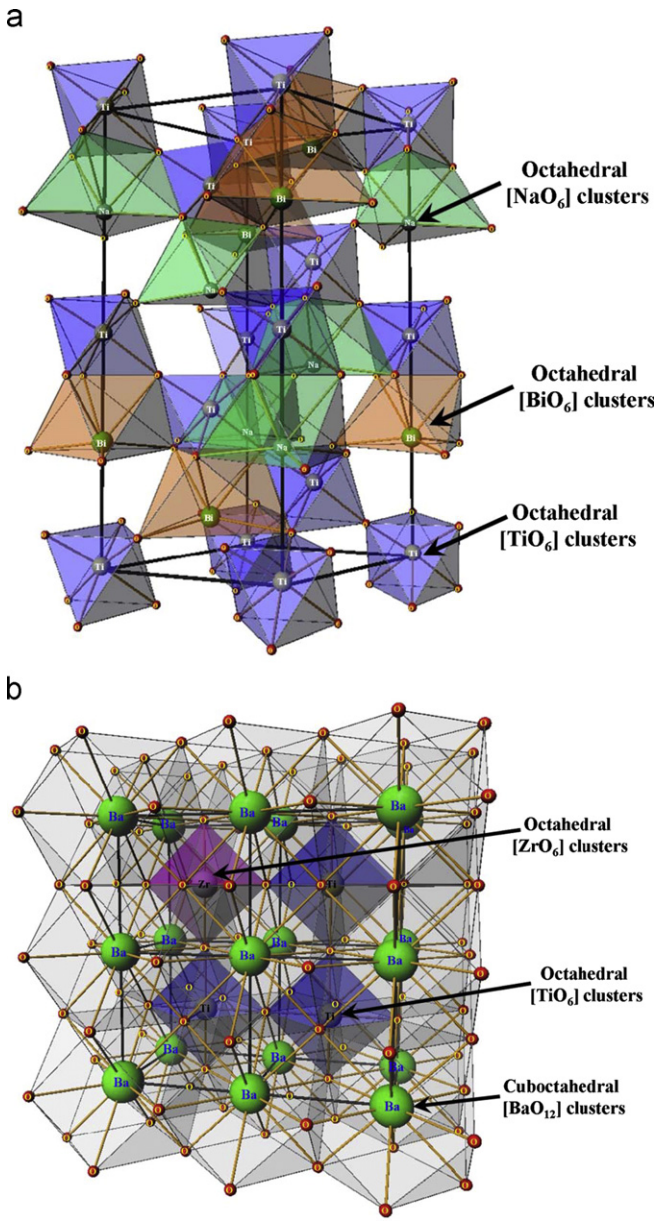

Fig. 3. Schematic representation of the unit cells for: (a) $(Bi_{0.5}Na_{0.5})TiO_3$ ceramics and supercells for the: (b) $Ba[Zr_{0.25}Ti_{0.75}]O_3$ ceramics.

Due to the disorder in the A-site related to distorted octahedral $[BiO_6]$ and $[NaO_6]$ clusters (Fig. 3(a)), this BNT ceramic with a rhombohedral structure has 13 Raman-active modes with the following representation: $\Gamma_{Raman}=4A_1+9E$ that have been analyzed and reported by Petzelt et al. [43]. The Raman peaks in Fig. 4 are relatively broad, which may be caused by distorted octahedral $[BiO_6]$ and $[NaO_6]$ clusters or disorder in the A-site of the rhombohedral structure. Also an overlap of Raman peaks is observed in all solid solutions. The first Raman-active $A_1(TO_1)$ mode at around (146 cm^{-1}) is related to network modifiers or distorted octahedral $[BiO_6]$ and $[NaO_6]$ clusters. The second Raman-active $E(TO_2)$ mode can be deconvoluted in three Raman peaks in 279 cm^{-1} regions. This mode is assigned to stretching arising from the bonds due to the presence of octahedral $[TiO_6]$ clusters at

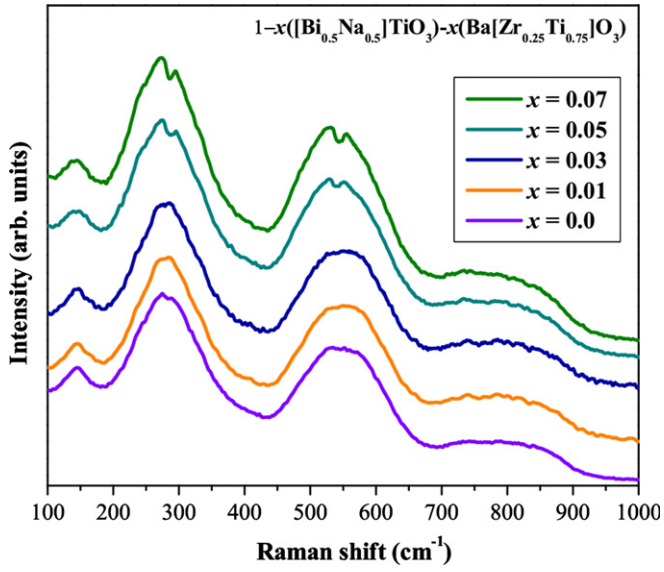

Fig. 4. Raman spectra of $1-x(Bi_{0.5}Na_{0.5})TiO_3-xBa[Zr_{0.25}Ti_{0.75}]O_3$ ceramics.

short-range. The mode shows anomaly at $x=0.05$ and starts splitting into two bands that shift apart with further increase in the BZT content. The third Raman-active (LO_2) mode with low intensity is related to short-range electrostatic forces associated with the lattice ionicity [44]. According to Domenico et al. [45], the (TO_3) mode situated at around 542 cm^{-1} is ascribed to the ($\leftarrow O\leftarrow Ti\rightarrow O\rightarrow$) stretching symmetric vibrations of the octahedral [TiO_6] clusters. This mode is common in materials with perovskite-type structure. However the spectral signature of the band shows a change at $x=0.05$ and separates into two distinct bands at $x=0.07$. Finally, the (LO_3) mode found at 812 cm^{-1} is due to the sites within the rhombohedral lattice containing octahedral distorted [TiO_6] clusters [46]. These modes are classified into longitudinal (LO) and transverse (TO) components due to their electronic structures with a polar lattice character. However, Fig. 4 shows that all the Raman peaks are very broad. This behavior is possible due to disordered structure or distorted octahedral [TiO_6] clusters at short-range in both rhombohedral-BNT and cubic-BZT lattices.

3.4. Microstructural analyses

Fig. 5(a–e) shows SEM images of the $1-x(BNT)-x(BZT)$ ceramic ($x=0$, 0.01, 0.03, 0.05 and 0.07) sintered at 1150 °C for 4 h. The pure BNT ceramics have a microstructure with rectangular grains, while the addition of BZT ceramic into the BNT matrix promotes a change to spherical grains (Fig. 5 (a–e)).The BNT disk appears to be poly-dispersed in both size and shape due to inhomogeneous grain growth. However, the addition of BZT ceramics results in the inhibition of grain growth, so the crystals of the BNT–BZT appear to be more uniform in both size and shape. Also the grain size is reduced with an increase in BZT content in compositions up to $x=0.03$ because Ba^{2+} is abundant in crystal boundary, which prevents the ion from migrating and restrains growth between grains. The SEM image confirms that $1-x(BNT)-x(BZT)$ ceramics are densely sintered and all compositions have high density at around 5.67–5.83 g/cm^3 which is more than 96% of the theoretical density. The Energy Dispersive X-ray Spectroscopy (EDS) of pure BNT and BNT–BZT compositions are shown in Fig. 6. The spectrum shows that all the elements are present with respect to their stochiomtery.

3.5. Dielectric properties analyses

Fig. 7 illustrates the temperature dependent dielectric behavior of $1-x(BNT)-x(BZT)$ ceramics with $x=0$, 0.01, 0.03, 0.05 and 0.07 at 100 kHz. It is seen from Fig. 6 that two dielectric peaks have been observed in each composition. The observed two dielectric peaks can be attributed to the factors caused by the phase transitions from ferroelectric to anti-ferroelectric, which is called depolarization temperature (T_d) and from anti-ferroelectric to paraelectric phase, at which the maximum value of dielectric constant corresponding temperature is the Curie temperature (T_m). The values of T_d and T_m are found to decrease with increase in the concentration of BZT, indicating that the conductivity of the materials is decreased compared with BNT. The MPB composition exhibits a lower depolarization temperature, which implies a reduction of the stability of ferroelectric domains. Compared with the compositions consisting of one single phase, the coexistence of a mixed rhombohedral– cubic phase could lead to more powerful stress in the MPB compositions, due to the incompatibility of their crystal lattices, resulting in a decrease of the thermal stability in the long-range ferroelectric domains [47]. The variation of dielectric constant (ε_r) with different x contents is given in Table 2. Moreover ε' increases with an increase of BZT ceramic up to $x=0.05$ and decreases with a further increase in the x (BZT) content. This behavior can be assigned to substitution of Na, Bi, and Ti atoms (with atomic radius: 186 pm, 156 pm and 147 pm respectively) by Ba and Zr atoms (with atomic radius: 222 and 160 pm respectively) [47,48]. The addition of BZT in the BNT matrix makes the lattice structure incompact which is favorable for domain wall motion [49], hence the relative permittivity increases. Again Ba^{2+} doping also leads to a series of space charge centers and these space charge centers can disorder the distribution of electric potential, which can increase the potential barrier and the migration of the ions is restrained [50,51]. Meanwhile, further increase of BZT ($x=0.07$) ceramic into the BNT matrix leads to a decline in ε_r due to possible reaction of oxygen vacancies ($V_O^{\bullet\bullet}$). When the BZT content reaches its limit, further addition saturates the BNT lattice matrix and causes the clamping of wall domain [52]. This clamping will restrain the macro–micro domain switching in some degree; this is the reason that the relative permittivity declined at $x=0.07$.

The temperature dependent dielectric study shows a broad peak at phase transition (T_c) temperature indicating that the

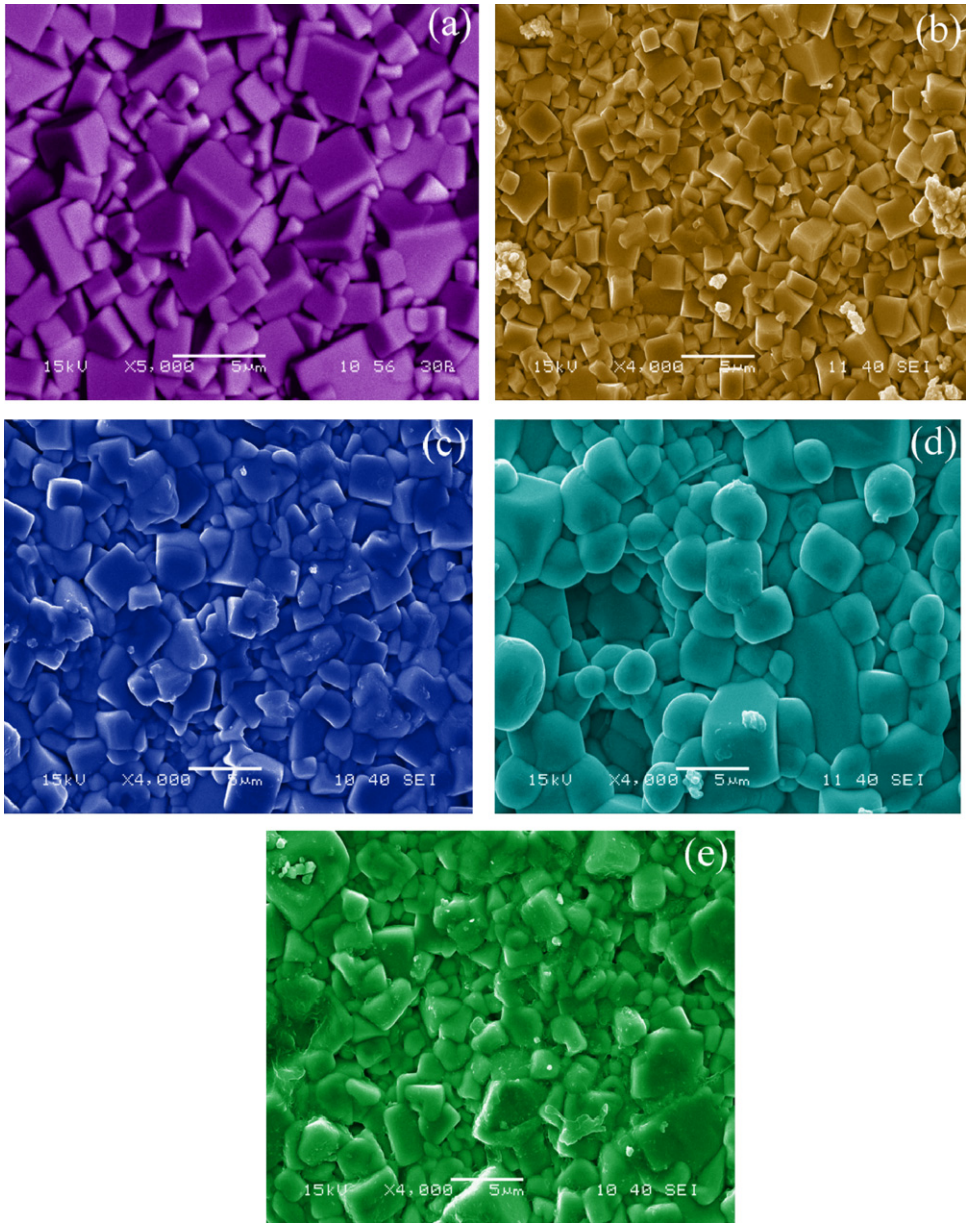

Fig. 5. SEM image for $1-x(Bi_{0.5}Na_{0.5})TiO_3-xBa[Zr_{0.25}Ti_{0.75}]O_3$ ceramics with $x=0$ (a); $x=0.01$ (b); $x=0.03$ (c); $x=0.05$ (d); and $x=0.07$ (e).

phase transition is a diffuse type. The broadening or diffuseness of the peak may be due to the substitution disordering in the arrangement of cations at one or more crystallographic sites in the lattice structure leading to heterogeneous domains or may be due to the defect induced relaxation at high temperature [53–55]. The diffusivity parameter is been calculated by modified Curie–Weiss law, in Eq. (1) [56,57].

$$\frac{1}{\varepsilon}-\frac{1}{\varepsilon_m}=\frac{(T-T_m)^{\gamma}}{C_1}\ldots(\mathbf{at}\ \ \boldsymbol{T>T_m}) \quad (1)$$

where γ and C_1 are constants for diffusion factor and Curie–Weiss constants, respectively. In general, the diffusion factor is between 1 and 2, representing the normal ferroelectric phase transition and diffuse phase transition. Plots of $\ln(1/\varepsilon'-1/\varepsilon_m)$ as a function of $\ln(T-T_m)$ for all compositions are shown in Fig. 8. The diffusion factor can be employed to describe the diffusion phase transition [58]. The diffusion factor compositional dependence is shown in Table 2. The diffusivity value increases with increase in BZT content indicating a relaxor behavior in the solid solution. The diffused phase transition behavior in BNT–BZT lead-free ceramics can be explained in terms of the coexistence of both polar rhombohedral structure and non-polar cubic structure with distorted octahedral $[TiO_6]$ clusters due to the cation disorder. In the BNT–BZT system Ba^{2+} and Zr^{4+} occupy A-site and B-site of ABO_3 perovskite structure respectively. In A-site Na, Bi and Ba have different valences and ionic radii, which results in the formation of the local electric fields owing to the local charge imbalance and the local elastic fields due to local structure distortions. Similar phenomenon also occurs at the B-site of

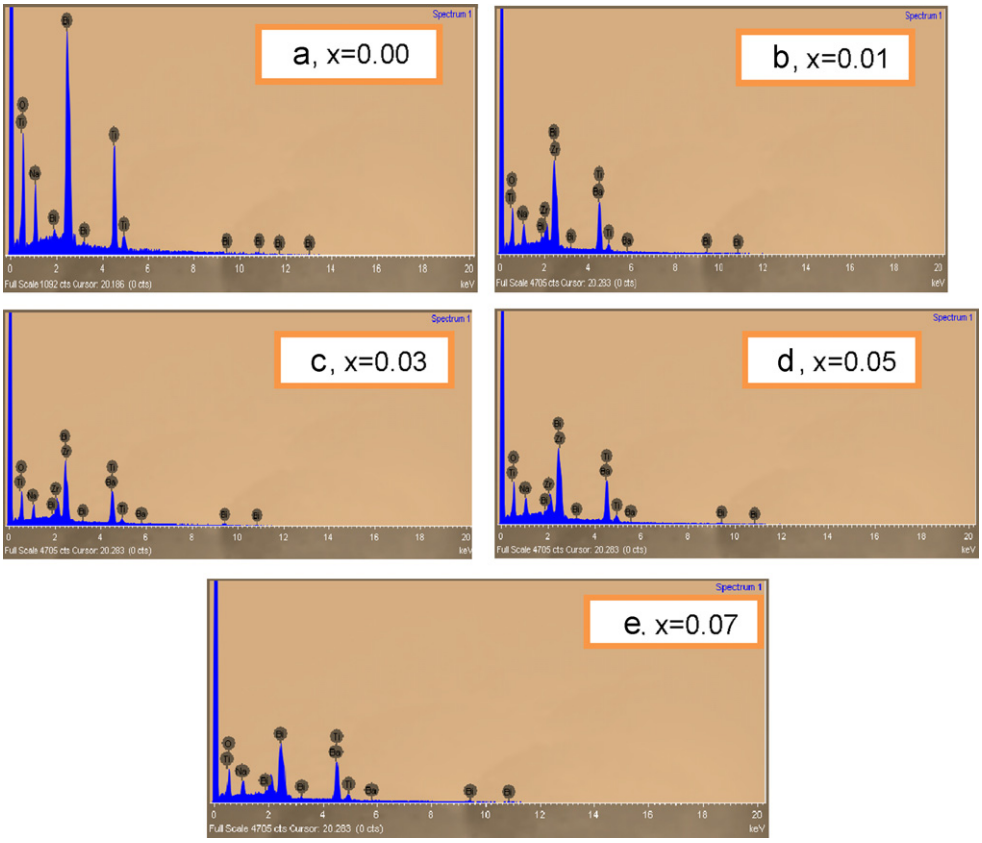

Fig. 6. EDS of $1-x(Bi_{0.5}Na_{0.5})TiO_3-xBa[Zr_{0.25}Ti_{0.75}]O_3$ ceramics with $x=0$ (a); $x=0.01$ (b); $x=0.03$ (c); $x=0.05$ (d); and $x=0.07$ (e).

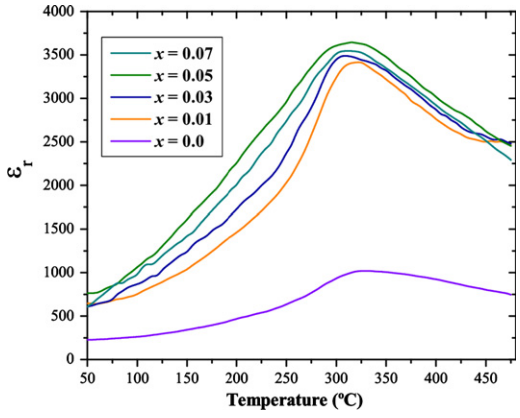

Fig.7. Temperature dependence dielectric study of $1-x(Bi_{0.5}Na_{0.5})TiO_3-x$ $Ba[Zr_{0.25}Ti_{0.75}]O_3$ ceramics at 100 kHz.

the ABO_3 perovskite structure. The presence of the random field including the local electric fields and elastic field hinders the long-range dipole alignment, i.e., giving rise to PNRs. These PNRs are isolated and frustrated in the system and are embedded in the disordered matrix, which results in the relaxor behavior. Consequently, the relaxor behavior of BNT–BZT ceramics is believed to result from the complex response of all the PNRs and matrices. Recently it was reported by Yao et al. [59] that the size of PNR decreases and the higher degree of self-organization increases as the composition approaches the MPB. Such self-organization indicates that the system is able to relax its elastic energy by geometrically arranging the PNRs into improper ferroelastic domain bands. Stress accommodated finer PNRs would result in a polydomain structure, which is more susceptible to electric field E. So the diffusivity in the dielectric spectrum is maximum at the MPB region.

3.6. Ferroelectric properties analyses

Fig. 9 shows P–E loops of $1-x(BNT)-x(BZT)$ ceramics with $x=0$; 0,01; 0.03; 0.05; and 0.07 with a maximum coercive field (E_c) of 42 kV/cm at room temperature.

In comparison with BNT ceramic, BNT–BZT ceramic shows an enhanced remanent polarization and coercive field, indicating a modification of ferroelectric properties. The variation in P_r and E_c is given in Table 1 which is related to structure parameters such as dc–a, α_R, and the cT/aT ratio. The value of E_c represents the difficulty of domain alignment, which is related to the degree of distortion of a unit cell. In general, a less distorted unit cell (i.e., close to a cube) usually accompanies a lower strain and a smaller E_c during domain alignment. The increase in E_c with increase in BZT content may be due to the increase of cT/aT ratio upto $x=0.05$. But a decrease in E_c occurs at $x=0.07$ due to the change of α_R toward 90°. The smallest E_c in the present system is found at $x=0.07$, a

Table 2
Dielectric, ferroelectric and piezoelectric coefficients of $1-x(Bi_{0.5}Na_{0.5})TiO_3-xBa[Zr_{0.25}Ti_{0.75}]O_3$ ceramics.

$1-x[Bi_{0.5}Na_{0.5}]TiO_3-x$ $Ba[Zr_{0.25}Ti_{0.75}]O_3$ ceramics	T_c (°C)	T_d	ε_m	γ	d_{33} (pC/N)	E_c (kV/cm)	P_r ($\mu C/cm^2$)
$x=0$	333	210	1020	1.4	41	20	2.5
$x=0.01$	327	190	3382	1.42	60	22.5	4.2
$x=0.03$	319	175	3427	1.47	87	25.2	5.8
$x=0.05$	310	155	3533	1.57	131	29.7	12
$x=0.07$	319	165	3416	1.42	113	12.6	5.7

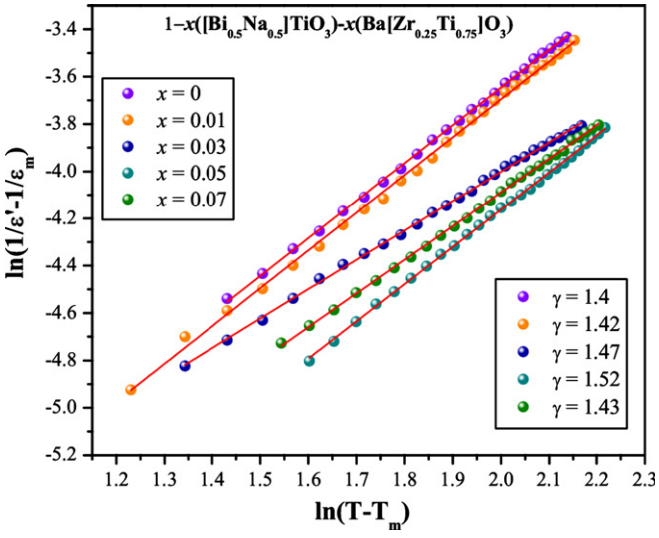

Fig. 8. $\ln(1/\varepsilon-1/\varepsilon_m)$ vs $(T-T_m)$ of $1-x(Bi_{0.5}Na_{0.5})TiO_3-xBa[Zr_{0.25}Ti_{0.75}]O_3$ ceramics at 100 kHz.

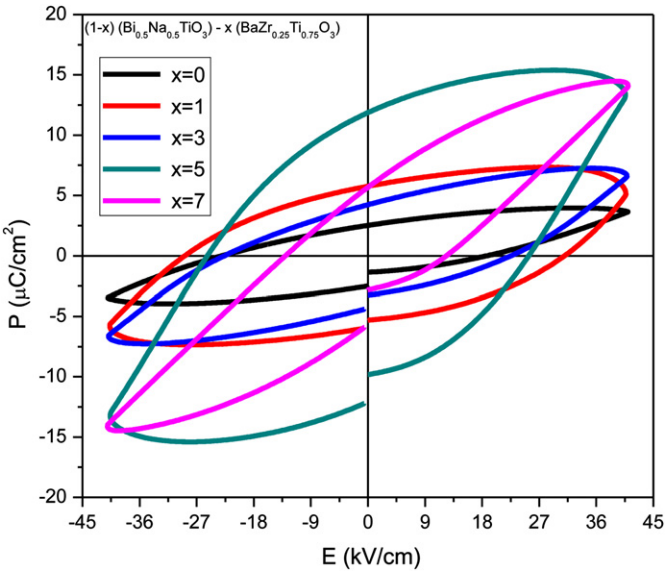

Fig. 9. The P–E hysteresis loops of $1-x(Bi_{0.5}Na_{0.5})TiO_3-xBa[Zr_{0.25}Ti_{0.75}]O_3$ ceramics.

cubic side of the MPB composition, but not at the MPB composition that also has been observed in other BNT-based ceramic systems [60,61]. Consequently, a significant decrease in Ec can be found in the BNT-based system as the composition is fully passing through the MPB region to the cubic phase, which also provides another method for determining the MPB composition. For the present work, an obvious decrease in Ec occurs from 5% to 7%, which reveals that $x=0.07$ is fully passing the MPB region. Therefore, $x=0.05$ is the MPB composition with coexisting rhombohedral and cubic phases, and that is in agreement with the crystal structure refinement result from the XRD pattern.

3.7. Piezoelectric properties analyses

Fig. 10 shows the compositional dependence of the piezoelectric coefficient d_{33} as a function of the xBZT fraction.

The piezoelectric coefficient d_{33} increases with increase in BZT content and attains a maximum value of 131 pC/N for $x=0.05$ in the MPB region and then decreases to 111 pC/N for $x=0.07$. The increase in the piezoelectric constant d_{33} in the MPB composition may be attributed to an increase in the domain wall flexibility. Our results

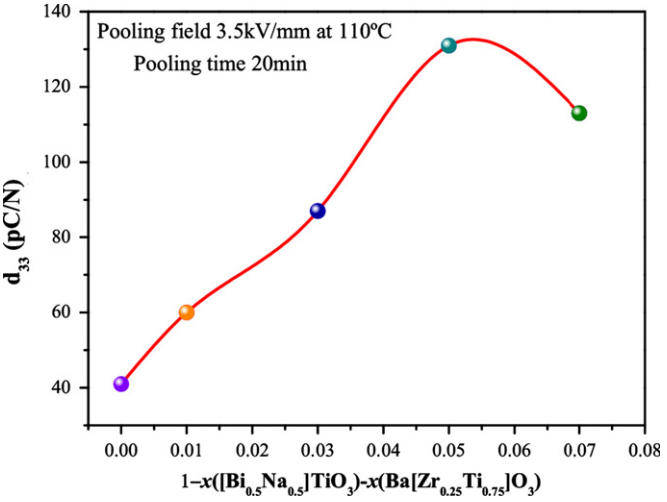

Fig. 10. Composition vs. d_{33} for the $1-x(Bi_{0.5}Na_{0.5})TiO_3-xBa[Zr_{0.25}Ti_{0.75}]O_3$ ceramics.

indicate that the BNT–BZT system (similar to PZT) has MPB, and thus it possesses stronger piezoelectric properties which is in agreement with results reported by Lin et al. [62]. The ceramics crystal structure is considered

to be a coexistence of rhombohedral and cubic phases in the MPB composition. As the rhombohedral phase free energy is close to the cubic phase free energy, these two phases are easily exchanged by applying an electric field. In the close vicinity of MPB both the crystallographic phases are in thermal equilibrium with each other with vanishing polarization anisotropy [63]. Therefore, a flipping of polarization between two phases is possible on application of electric field. Enhanced piezoelectric coefficients are obtained in MPB regions and are attributed to an easy switch in the polarization vector between all allowed polarization orientations [64,65].

4. Conclusions

In summary, the BNT-based solid solution $1-x$(BNT)$-x$ (BZT) ceramics with $x=0$; 0,01; 0.03; 0.05 and 0.07 were prepared by the solid state reaction method. The MPB of rhombohedral and cubic phases was detected in the range at $x=0.05$ by the XRD patterns and Rietveld refinement data. Raman spectroscopy also indicated the presence of MPB in the solid solution. Enhanced electrical properties have been obtained at the MPB region with maximum dielectric constant, spontaneous polarization, coercive field and piezoelectric constant. In the MPB region, the polarization vector can easily switch (upon application of a small field) between all the allowed polarization orientations, and hence enhances the dielectric constant, and ferroelectric and piezoelectric coefficients. So the BNT–BZT system is expected to be a new and promising candidate for lead-free dielectric and piezoelectric material

Acknowledgments

The authors thank the financial support of the Brazilian research financing institutions: CNPq (159710/2011-1), the FAPESP-Postdoctorate (No. 2009/50303-4), CAPES and FAPEPI-GERATEC (No. 01.08.0506.00).

References

[1] T. Takenaka, H. Nagata, Current status and prospects of lead-free piezoelectric ceramics, Journal of the European Ceramic Society 25 (2005) 2693–2700.
[2] T.R. Shrout, S.J. Zhang, Lead-free piezoelectric ceramics: Alternatives for PZT?, Journal of Electroceramics 19 (2007) 113–126
[3] J. Rödel, W. Jo, K.T.P. Seifert, E.-M. Anton, T. Granzow, D. Damjanovic, Perspective on the development of lead-free piezoceramics, Journal of the American Ceramic Society 92 (2009) 1153–1177.
[4] P.K. Panda, Review: environmental friendly lead-free piezoelectric materials, Journal of Materials Science 44 (2009) 5049–5062.
[5] Y.-Q. Lu, Y.-X. Li, A review on lead-free piezoelectric ceramics studies in China, Journal of Advanced Dielectrics 01 (2011) 269–288.
[6] G.A. Smolenskii, V.A. Isupov, A.I. Agranovskaya, N.N. Kranik, New ferroelectric of complex composition. 4., Sov, Physics of the Solid State 2 (1961) 2651–2654.
[7] C.F. Buhrer, Some properties of bismuth perovskites, The Journal of Chemical Physics 36 (1962) 798–805.
[8] V.A. Isupov, I.P. Pronin, T.V. Krunina, Temperature dependence of bireringence and opalescence of the sodium-bismuth titanate crystals, Ferroelectrics Letters Section 2 (1984) 205–208.
[9] J. Suchanicz, K. Roleder, A. Kania, J. Handerek, Electrostrictive strain and pyroeffect in the region of phase coexistence in $Na_{0.5}Bi_{0.5}TiO_3$, Ferroelectrics 77 (1988) 107–110.
[10] S.A. Sheets, A.N. Soukhojak, N. Ohashi, Y.M. Chiang, Relaxor single crystals in the $(Bi_{1/2}Na_{1/2})_{1-x}Ba_xZr_yTi_{1-y}O_3$ system exhibiting high electrostrictive strain, Journal of Applied Physics 90 (2001) 5287–5295.
[11] M.S. Hagiyev, I.H. Ismailzade, A.K. Abiyev, Pyroelectric properties of $(Na_{1/2}Bi_{1/2})TiO_3$ ceramics, Ferroelectrics 56 (1984) 215–217.
[12] S.E. Park, S.J. Chung, I.T. Kim, K.S. Hong, Nonstoichiometry and the long-range cation ordering in crystals of $(Na_{1/2}Bi_{1/2})TiO_3$, Journal of the American Ceramic Society 77 (1994) 2641–2647.
[13] I.P. Pronin, P.P. Syrnikov, V.A. Isupov, V.M. Egorov, N.V. Zaitseva, A.F. Jaffe, Peculiarities of phase-transitions in sodium–bismuth titanate, Ferroelectrics 25 (1980) 395–397.
[14] S.E. Park, K.S. Hong, Phase relations in the system of $(Na_{1/2}Bi_{1/2})TiO_3$–$PbTiO_3$. I. Structure, Journal of Applied Physics 79 (1996) 383–387.
[15] T.V. Kruznia, V.V. Gene, V.A. Isupov, E.V. Sinyakov, A change in birefringence on phase-transitions in $Na_{0.5}Bi_{0.5}TiO_3$ single-crystals, Kristallografiya 26 (1981) 852–854.
[16] T. Takenaka, K. Sakata, Dielectric, piezoelectric and pyroelectric properties of $(BiNa)_{1/2}TiO_3$-based ceramics, Ferroelectrics 95 (1989) 153–156.
[17] T. Takenaka, K. Sakata, K. Toda, Piezoelectric properties of $(Bi_{1/2}Na_{1/2})TiO_3$-based ceramics, Ferroelectrics 106 (1990) 375–380.
[18] Y. Hiruma, Y. Imai, Y. Watanabe, H. Nagata, T. Takenaka, Large electrostrain near the phase transition temperature of $(Bi_{0.5}Na_{0.5})TiO_3$–$SrTiO_3$ ferroelectric ceramics, Applied Physics Letters 92 (2008) 262904–262906.
[19] T. Takenaka, H. Nagata, Present status of non-lead-based piezoelectric ceramics, Key Engineering Materials 157 (1999) 57–63.
[20] A. Sasaki, T. Chiba, Y. Mamiya, E. Otsuki, Dielectric and piezoelectric properties of $(Bi_{0.5}Na_{0.5})TiO_3$–$(Bi_{0.5}K_{0.5})TiO_3$ systems, Japanese Journal of Applied Physics 38 (1999) 5564–5567.
[21] X.X. Wang, S.H. Choy, X.G. Tang, H.L.W. Chan, Dielectric behavior and microstructure of $(Bi_{1/2}Na_{1/2})TiO_3$–$(Bi_{1/2}K_{1/2})TiO_3$–$BaTiO_3$ lead-free piezoelectric ceramics, Journal of Applied Physics 97 (2005) 104101–104104.
[22] S.E. Park, S. Wada, L.E. Cross, T.R. Shrout, Crystallographically engineered $BaTiO_3$ single crystals for high-performance piezoelectrics, Journal of Applied Physics 86 (1999) 2746–2750.
[23] Z. Yu, R.Y. Guo, A.S. Bhalla, Orientation dependence of the ferroelectric and piezoelectric behavior of $Ba(Ti_{1-x}Zr_x)O_3$ single crystals, Applied Physics Letters 77 (2000) 1535–1537.
[24] C. Ang, Z. Yu, Z. Jing, R.Y. Guo, A.S. Bhalla, Piezoelectric and electrostrictive strain behavior of Ce-doped $BaTiO_3$ ceramics, Applied Physics Letters 80 (2002) 3424–3426.
[25] Y. Zhi, A. Chen, R. Guo, A.S. Bhalla, Dielectric properties and high tunability of $Ba(Ti_{0.7}Zr_{0.3})O_3$ ceramics under dc electric field, Applied Physics Letters 81 (2002) 1285–1287.
[26] T. Badapanda, S.K. Rout, L.S. Cavalcante, J.C. Sczancoski, S. Panigrahi, E. Longo, M.S. Li, Optical and dielectric relaxor behaviour of $Ba(Zr_{0.25}Ti_{0.75})O_3$ ceramic explained by means of distorted clusters, Journal of Physics D: Applied Physics 42 (2009) 175414–175422.
[27] C.H. Wang, Physical and electric properties of lead-free $(Bi_{0.5}Na_{0.5})TiO_3$–Ba $(Zr_{0.04}Ti_{0.96})O_3$ ceramics near the morphotropic phase boundary, Journal of the Ceramic Society of Japan 116 (2008) 632–636.
[28] 〈http://www.ing.unitn.it/∼maud/〉.
[29] L. Lutterotti, S. Matthies, H.R. Wenk, MAUD: A Friendly Java Program for Material Analysis Using Diffraction, IUCr: Newsletter of the CPD. 21 1999, pp. 14–15.

[30] L. Lutterotti, M. Bortolotti, Object oriented programming and fast computation techniques in Maud, a program for powder diffraction analysis written in java, IUCr: CompComm Newsletter 1 (2003) 43–50.
[31] H.M. Rietveld, A profile refinement method for nuclear and magnetic structures, Journal of Applied Crystallography 2 (1969) 65–71.
[32] L. Lutterotti, S. Matthies, D. Chateigner, S. Ferrari, J. Ricote, Rietveld texture and stress analysis of thin films by X-ray diffraction, Materials Science Forum 408 (2002) 1603–1608.
[33] Y. Xie, L. Lutterotti, H.R. Wenk, F. Kovacs, Texture analysis of ancient coins with TOF neutron diffraction, Journal of Materials Science 39 (2004) 3329–3337.
[34] R. Ranjan, A. Dviwedi, Structure and dielectric properties of $(Na_{0.50}Bi_{0.50})_{1-x}Ba_xTiO_3$: $0 \le x \le 0.10$, Solid State Communications 135 (2005) 394–399.
[35] J. Joseph, T.M. Vimala, J. Raju, V.R.K. Murthy, Structural investigations on the (Ba,Sr)(Zr,Ti)O_3 system, Journal of Physics D: Applied Physics 32 (1999) 1049–1057.
[36] T. Badapanda, V. Senthil, S.K. Rout, L.S. Cavalcante, A.Z. Simões, T.P. Sinha, S. Panigrahi, M.M. de Jesus, E. Longo, J.A. Varela, Rietveld refinement, microstructure, conductivity and impedance properties of $Ba[Zr_{0.25}Ti_{0.75}]O_3$ ceramic, Current Applied Physics 11 (2011) 1282–1293.
[37] K. Momma, F. Izumi, VESTA 3 for three-dimensional visualization of crystal, volumetric and morphology data, Journal of applied crystallography 44 (2011) 1272–1276.
[38] R. Bujakiewicz-Koronska, Y. Natanzon, Determination of elastic constants of $Na_{0.5}Bi_{0.5}TiO_3$ from ab initio calculations, Phase Transformations 81 (2008) 1117–1124.
[39] 〈http://en.wikipedia.org/wiki/Octahedron〉.
[40] 〈http://en.wikipedia.org/wiki/Cuboctahedron〉.
[41] D. Rout, K.S. Moon, S.J.L. Kang, I.W. Kim, Dielectric and Raman scattering studies of phase transitions in the $(100-x)Na_{0.5}Bi_{0.5}TiO_3$–$xSrTiO_3$ system, Journal of Applied Physics 108 (2010) 084102–084108.
[42] B.W.V. Eerd, D. Damjanovic, N. Klein, N. Setter, J. Trodahl, Structural complexity of $(Na_{0.5}Bi_{0.5})TiO_3$–$BaTiO_3$ as revealed by Raman spectroscopy, Physical Review B 82 (2010) 104112–104118.
[43] J. Petzelt, S. Kamba, J. Fábry, D. Noujni, V. Porokhonskyy, A. Pashkin, I. Franke, K. Roleder, J. Suchanicz, R. Klein, G.E. Kugel, Infrared, Raman and high-frequency dielectric spectroscopy and the phase transitions in $Na_{1/2}Bi_{1/2}TiO_3$, Journal of Physics Condensed Matter 16 (2004) 2719–2731.
[44] A. Chaves, R.S. Katiyar, S.P.S. Porto, Coupled modes with A1 symmetry in tetragonal $BaTiO_3$, Physical Review B 10 (1974) 3522–3533.
[45] M.D. Domenico Jr., S.H. Wemple, S.P.S. Porto, P.R. Buman, Raman spectrum of single-domain $BaTiO_3$, Physical Review 174 (1968) 522–530.
[46] J.C. Sczancoski, L.S. Cavalcante, T. Badapanda, S.K. Rout, S. Panigrahi, V.R. Mastelaro, J.A. Varela, M.S. Li, E. Longo, Structure and optical properties of $[Ba_{1-x}Y_{2x/3}](Zr_{0.25}Ti_{0.75})O_3$ powders, Solid State Sciences 12 (2010) 1160–1167.
[47] D.L. West, D.A. Payne, Preparation of $0.95Bi_{1/2}Na_{1/2}TiO_3 \cdot 0.05$ $BaTiO_3$ ceramics by an aqueous citrate–gel route, Journal of the American Ceramic Society 86 (2003) 769–744.
[48] V.S. Puli, A. Kumar, D.B. Chrisey, M. Tomozawa, J.F. Scott1, R.S. Katiyar, Barium zirconate–titanate/barium calcium-titanate ceramics via sol–gel process: novel high-energy-density capacitors, Journal of Physics D: Applied Physics 44 (2011) 395403–395412.
[49] H. Zhang, D. Jin, Preparation and ferroelectric properties of lead-free $Bi_{0.5}Na_{0.5}TiO_3$–$BaTiO_3$ ceramics synthesized with citrate method, Advances in Materials Research 485 (2012) 271–274.
[50] R.D. Roseman, N. Mukherjee, PTCR effect in $BaTiO_3$: Structural aspects and grain boundary potentials, Journal of Electroceramics 10 (2003) 117–135.
[51] L.S. Cavalcante, M.F.C. Gurgel, E.C. Paris, A.Z. Simões, M.R. Joya, J.A. Varela, P.S. Pizani, E. Longo, Combined experimental and theoretical investigations of the photoluminescent behavior of $Ba(Ti,Zr)O_3$ thin films, Acta Materialia 55 (2007) 6416–6426.
[52] Y. Qu, D. Shan, J. Song, Effect of A-site substitution on crystal component and dielectric properties in $Bi_{0.5}Na_{0.5}TiO_3$ ceramics, Materials Science and Engineering B 121 (2005) 148–151.
[53] Y. Kitanaka, Y. Noguchi, M. Miyayama, Oxygen-vacancy-induced 90°-domain clamping in ferroelectric $Bi_4Ti_3O_{12}$ single crystals, Physical Review B 81 (2010) 094114–094121.
[54] K.S. Hong, S.E. Park, Journal of Applied Physics 79 (1996) 388–392.
[55] J. Li, F. Wang, X. Qin, M. Xu, W. Shi, Large electrostrictive strain in lead-free $Bi_{0.5}Na_{0.5}TiO_3$–$BaTiO_3$–$KNbO_3$ ceramics, Applied Physics A 104 (2011) 117–122.
[56] N. Majlis, The Quantum Theory of Magnetism, World Scientific, Singapore, 2003, pp. 35.
[57] D.C. Mattis, The Theory of Magnetism Made Simple: An Introduction To Physical Concepts and To Some Useful Mathematical Methods, World Scientific, Singapore, 2006, pp. 25–30.
[58] T. Badapanda, S.K. Rout, L.S. Cavalcante, J.C. Sczancoski, S. Panigrahi, T.P. Sinha, E. Longo, Structural and dielectric relaxor properties of yttrium-doped $Ba(Zr_{0.25}Ti_{0.75})O_3$ ceramics, Materials Chemistry and Physics 121 (2010) 147–153.
[59] J. Yao, N. Monsegue, M. Murayama, W. Leng, W.T. Reynolds, Q. Zhang, H. Luo, J. Li, W. Ge, D. Viehland, Role of coexisting tetragonal regions in the rhombohedral phase of $Na_{0.5}Bi_{0.5}TiO_3$–x at% $BaTiO_3$ crystals on enhanced piezoelectric properties on approaching the morphotropic phase boundary, Applied Physics Letters 100 (2012) 012901.
[60] J. Shieh, K.C. Wu, C.S. Chen, Switching characteristics of MPB compositions of $(Bi_{0.5}Na_{0.5})TiO_3$–$BaTiO_3$–$(Bi_{0.5}K_{0.5})TiO_3$ lead-free ferroelectric ceramics, Acta Materialia 55 (9) (2007) 3081–3087.
[61] C. Peng, J.F. Li, W. Gone, Preparation and properties of $(Bi_{1/2}Na_{1/2})TiO_3$–$Ba(Ti,Zr)O_3$ lead-free piezoelectric ceramics, Materials Letters 59 (2005) 1576–1580.
[62] D. Lin, C. Xu, Q. Zheng, Y. Wei, D. Gao, Piezoelectric and dielectric properties of $Bi_{0.5}Na_{0.5}TiO_3$–$Bi_{0.5}Li_{0.5}TiO_3$ lead-free ceramics, Journal of Materials Science: Materials in Electronics 20 (2009) 393–397.
[63] P. Jaita, A. Watcharapasorn, S. Jiansirisomboon, Investigation of a new lead-free $Bi_{0.5}(Na_{0.40}K_{0.10})TiO_3$–$(Ba_{0.7}Sr_{0.3})TiO_3$ piezoelectric ceramic, Nanoscale Research Letters 7 (2012) 24–29.
[64] C. Peng, J.F. Li, W. Gong, Preparation and properties of $(Bi_{1/2}Na_{1/2})TiO_3$–$Ba(Ti,Zr)O_3$ lead-free piezoelectric ceramics, Materials Letters 59 (2005) 1576–1580.
[65] P. Kubelka, F. Munk–Aussig, Ein beitrag zur optik der farbanstriche, Fakultät für Technische Physik 12 (1931) 593–601.